

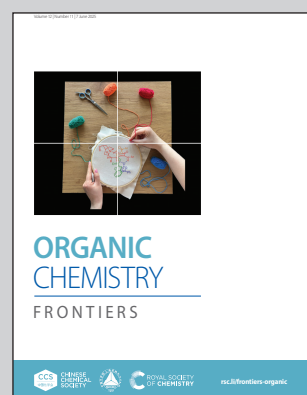
Showcasing research from Professor Bappaditya Gole's laboratory, Department of Chemistry, Shiv Nadar Institution of Eminence, Delhi NCR, India.

Unveiling stereoselective ladders *via* photo-oligomerization of a diazaanthracene macrocycle

Stereoselective oligomers are synthesized by leveraging steric interactions at remote sites from a photoresponsive macrocycle *via* [4 + 4] cycloaddition. Oligomers up to octamer were isolated and characterized. They retain reactivity to undergo further oligomerization, either independently or with fresh monomers.

Image reproduced by permission of Bappaditya Gole from *Org. Chem. Front.*, 2025, **12**, 3336.

As featured in:



See Bappaditya Gole *et al.*,  
*Org. Chem. Front.*, 2025, **12**, 3336.

Registered charity number: 207890

RESEARCH ARTICLE

[View Article Online](#)  
[View Journal](#) | [View Issue](#)



Cite this: *Org. Chem. Front.*, 2025, **12**, 3336

## Unveiling stereoselective ladders *via* photo-oligomerization of a diazaanthracene macrocycle†

Jinti Moni Kumar, <sup>a</sup> Ivan Huc, <sup>b</sup> Yann Ferrand <sup>c</sup> and Bappaditya Gole <sup>a\*</sup>

We present an efficient light-driven oligomerization of a flat aromatic tetra-amide macrocycle containing photoresponsive 1,8-diazaanthracenes. Oligomers with molecular weights exceeding 10 kDa were straightforwardly obtained, isolated using gel permeation chromatography (GPC), and characterized by NMR and mass spectrometry up to an octamer. We finely tuned the side chain size to exclusively favor the *exo*-[4 + 4] photoadduct over the *endo*-[4 + 4] photoadduct, thus controlling the stereoselectivity of the photoreaction to produce a single isomer, which yielded ladder-like architectures. The octamer is a ~10 nm long ladder with a step size of 4.6 Å. The oligomers retained sufficient photoreactivity to undergo further oligomerization, either between themselves or upon adding fresh monomers, to generate longer oligomers. These oligomers are fully degradable as thermal reversibility allows for monomer recovery.

Received 23rd January 2025,  
Accepted 25th March 2025

DOI: 10.1039/d5q000159e

[rsc.li/frontiers-organic](http://rsc.li/frontiers-organic)

## Introduction

The emergence of covalent organic frameworks (COFs),<sup>1–7</sup> covalent organic cages,<sup>8–14</sup> and other carbon-rich materials<sup>15–24</sup> with fascinating properties has inspired chemists to explore simple synthetic methods useful for accessing such materials, starting with monomers encoded with functional information. Light-driven reactions, particularly polymerization, have proven to be efficient, mostly clean, environmentally friendly methods for producing functional materials.<sup>25–28</sup> However, in homogeneous solutions, the persistent challenge of achieving stereoselectivity and specificity continues to exist, primarily due to the difficulty of controlling the reactivity of the excited state, thus leading to products that are challenging to distinguish and separate. This issue was partially addressed by employing noncovalent supramolecular interactions and performing photochemical reactions in the solid state, taking benefit of their preorganization.<sup>29–35</sup> For example, the [4 + 4] photocycloaddition of anthracene derivatives, often exploited in supramolecular chemistry to create functional materials, is known to generate multiple regio- and stereoisomers in solution.<sup>36–43</sup> The 9- and 10-substituted

anthracenes give two stereoisomers, *syn* and *anti*, of different proportions depending on the substitution. The number of isomers increases if the substitution is present in any other position.<sup>44</sup> However, recently, several anthracene-based macrocycles and cages were considered as starting building blocks for the preparation of highly ordered, stereoselective two-dimensional porous polymers and membranes in a single-crystal-to-single-crystal transformation.<sup>45–49</sup> These studies primarily leverage monomer preorganization in a crystal or on a surface. Yet, attempts to achieve similar outcomes in solution have rarely been successful. A recent study employed time-resolved NMR spectroscopy to gain comprehensive insights into the polymerization of bis-anthracene monomers in solution but did not focus on isolating the resulting materials.<sup>50</sup> Control over the reactivity of the monomer would not only offer a method to regio- and stereoselectively produce polymers in solution without relying on the crystallization of the monomer in a preorganized fashion, but it would also provide opportunities for mechanistic studies by isolating intermediate oligomers, which form at the early stage of the reaction. Furthermore, oligomers may offer functional properties akin to those of polymers while offering better solubility, making them suitable for various solution-based techniques.<sup>51–53</sup>

Herein, we explore the photochemical reaction of planar aromatic tetra-amide macrocycle **1** containing 1,8-diazaanthracene units in solution. Unlike anthracene, which typically yields mixtures,<sup>36–43</sup> 1,8-diazaanthracenes (*i.e.*, pyrido-[3,2-*g*] quinolines) are known to produce exclusively the antiparallel photoproduct in solution to minimize dipolar repulsion (Fig. 1a) unless some constraints are applied to maintain the parallel arrangement of the reacting diazaanthracenes. In this case, the parallel photoproduct is quantitatively formed

<sup>a</sup>Biomimetic Supramolecular Chemistry Laboratory, Department of Chemistry, School of Natural Sciences, Shiv Nadar Institution of Eminence Deemed to be University, Greater Noida, Uttar Pradesh 201314, India.

E-mail: [bappaditya.gole@snu.edu.in](mailto:bappaditya.gole@snu.edu.in)

<sup>b</sup>Department of Pharmacy, Ludwig-Maximilians-Universität München, Butenandtstr. 5–13, 81377 Munich, Germany

<sup>c</sup>Univ. Bordeaux, CNRS, Bordeaux INP, CBMN, UMR 5248, F-33600 Pessac, France

† Electronic supplementary information (ESI) available. See DOI: <https://doi.org/10.1039/d5q000159e>



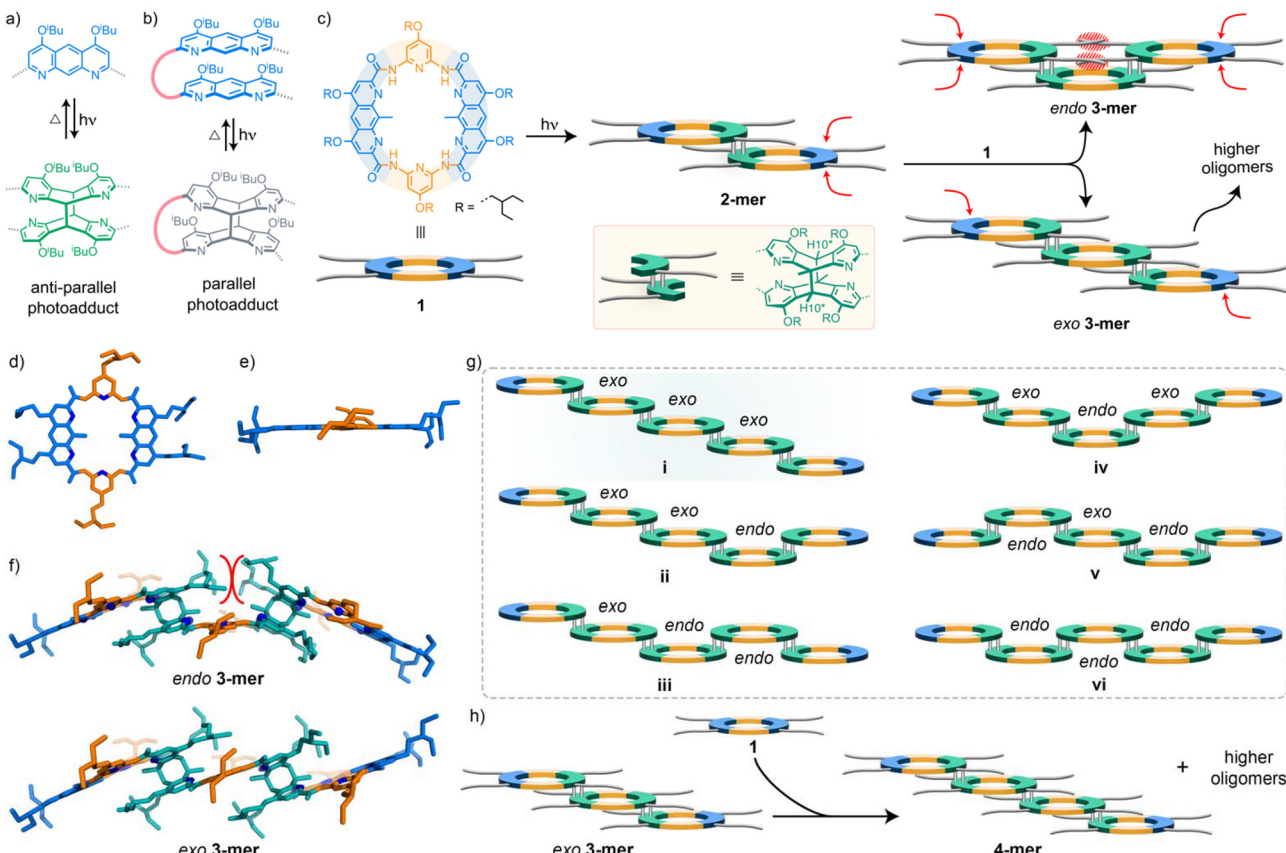


**Fig. 1** Schematic illustration of the (a) intermolecular and (b) intramolecular [4 + 4] photocycloadditions of 1,8-diazaanthracene that give anti-parallel and parallel photoadducts, respectively. (c) Chemical structure of macrocycle **1** and the schematic representation of its intermolecular [4 + 4] cycloaddition. In principle, upon chain elongation, different stereoisomers may form depending on the relative orientation of the approaching monomers (red arrows). However, 2-ethyl butoxy solubilizing side chains have been chosen to produce the exo-isomer selectively. The red scribbles in the *endo* 3-mer highlight possible steric hindrance, which does not allow two monomers to approach a macrocycle from the same side. (d) Top and (e) side views of the geometry-optimized structure of **1** highlighting its planar structure. (f) Energy-minimized models (Merck Molecular Force Field static, MMFFs) of two possible stereoisomers, *endo* 3-mer and *exo* 3-mer. Steric hindrance is highlighted with red lines. (g) As a representative example, a 5-mer can have six possible stereoisomers: the all *exo*, i.e., isomer **i**, forms selectively due to the size of the side-chains. (h) Schematic illustration showing the chain growth mechanism, where a trimer, for example, can be photoirradiated in the presence of fresh monomers to produce higher oligomers.

(Fig. 1b).<sup>54–61</sup> We show that macrocycle **1** undergoes intermolecular antiparallel [4 + 4] cycloaddition at both ends to create oligomers upon irradiation with UV light in chloroform (Fig. 1c). We have isolated oligomers of varying lengths with molecular weights of up to 10 kDa, allowing for their individual characterization. The photochemical reaction exclusively produced *exo*-[4 + 4] photoadducts and no *endo* isomer, thus providing a single isomer for each oligomer among multiple possibilities. Unlike conventional methods, which often rely on steric interactions near the reactive center to control, *e.g.*, iso- or syndiotactic polymer architectures,<sup>62,63</sup> the stereoselectivity in this system is governed by the manipulation of steric interactions at remote sites. The rigid structure of the macrocycle ensures that the resulting oligomers adopt a stiff, ladder-like architecture. Furthermore, we demonstrate that the shorter oligomers retain sufficient photoreactivity to undergo further oligomerization, either with themselves or with freshly added monomers, to generate longer oligomers (Fig. 1h).

## Results and discussion

The shape-persistent tetra-amide macrocycle **1** was prepared from 1,8-diazaanthracene-2,7-dicarboxylic acid and 2,6-diaminopyridine derivatives in a single-step amide coupling reaction in 33% yield (Schemes S1–S3 and Fig. S1 and S2†). Geometry optimization by density functional theory (DFT) calculations revealed that **1** adopts a planar rigid structure suitable for photoproduct formation at the 1,8-diazaanthracene sites (Fig. 1d and e).

In addition to their role in solubilizing the macrocycles, we have identified the possibility for side chains in positions 4 and 5 of the diazaanthracene to control the stereoselectivity of the oligomers. For instance, when a monomer approaches a 2-mer, two stereoisomers may form: an *endo* 3-mer and an *exo* 3-mer (Fig. 1c). We reasoned that the formation of the *endo*-isomer could be prevented by using sufficiently hindering side chains that would cause steric clashes only in the *endo*

pathway, *i.e.* the transition state (TS) energy of the *endo* 3-**mer** is expected to be reasonably higher than that of the *exo* 3-**mer**, leading to the stereoselective formation of the *exo* isomer (Fig. S3†). The energy-minimized models of the two possible 3-**mer** stereoisomers bearing 2-ethyl butoxy side chains showed that the *exo* 3-**mer** is stabilized by  $15 \text{ kJ mol}^{-1}$  compared to the *endo* 3-**mer**, which imposes a substantial strain on the central macrocycle to accommodate the bulky side chains (Fig. 1f). The energy-minimized structure showed that the strain on the central unit is reduced with smaller side chains, such as

methoxy or isobutoxy, which may alter the stereoselectivity (Fig. S3†). Furthermore, using smaller side chains would reduce the solubility drastically. We thus decided to use 2-ethyl butoxy side chains to both overcome solubility issues and achieve stereoselectivity. As illustrated in Fig. 1g, the 5-**mer** may exist as six possible stereoisomers. However, with our design strategy, only isomer **i** displaying four *exo*-bridges would be obtained. With increasing oligomer size, the number of possible stereoisomers increases; for example, it can be as high as 36 in the case of the octamer (Fig. S4†). Therefore,

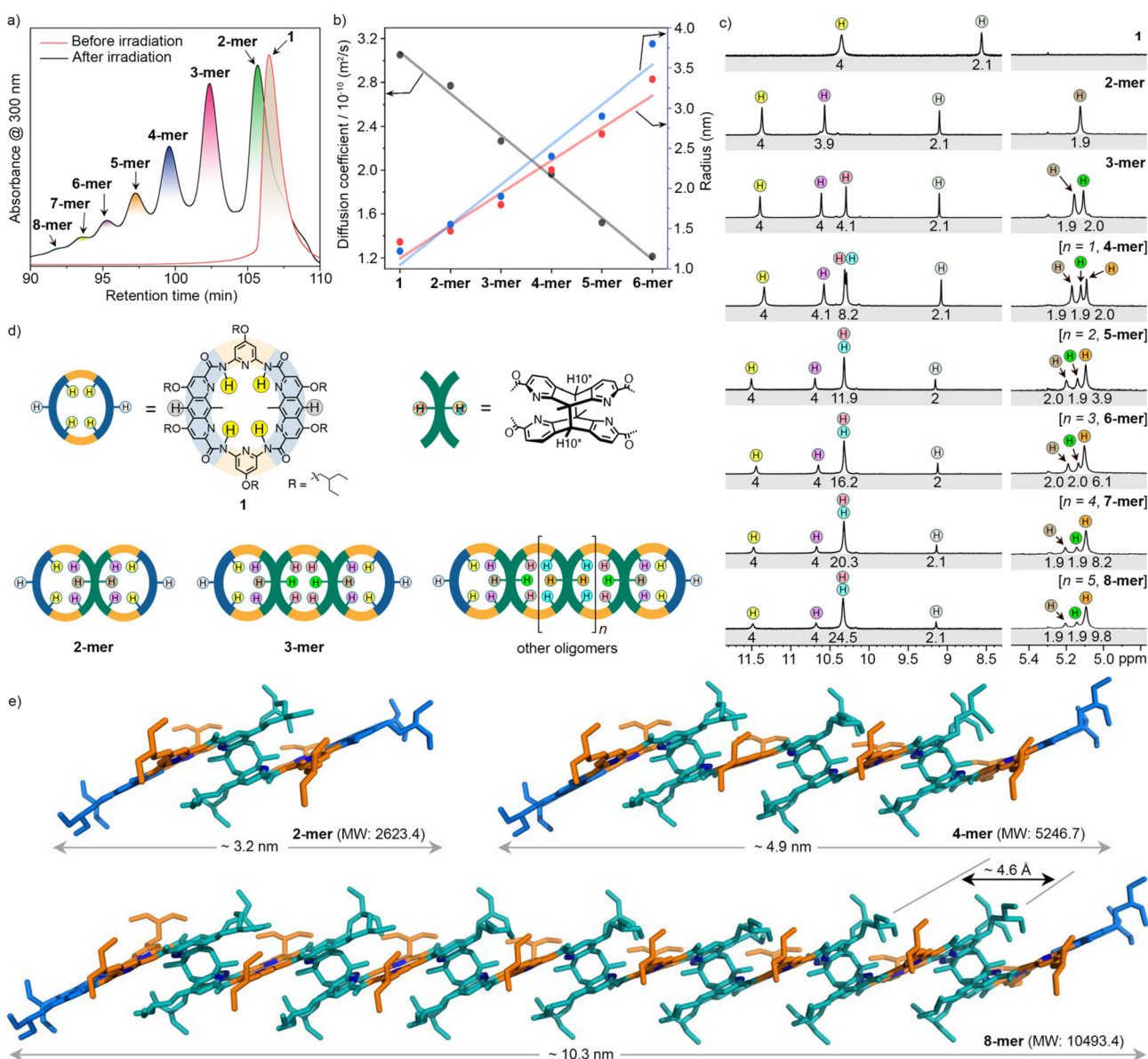


**Fig. 2** (a) Recycling preparative GPC profiles after three cycles ( $\text{CHCl}_3$ ,  $25^\circ\text{C}$ ,  $7 \text{ mL min}^{-1}$ ) before and after photoirradiation of **1** in  $\text{CHCl}_3$  showing a clear separation of oligomers of different sizes. (b) Diffusion coefficients (in grey) and corresponding solvodynamic radii (in red) of **1** and oligomers obtained from  $^1\text{H}$  DOSY experiments. The calculated radius (in blue) of the geometry-optimized oligomers is given for comparison. (c) Selected areas of  $^1\text{H}$ -NMR spectra (400 MHz, 298 K) in  $\text{CDCl}_3$  of **1** and the oligomers with relative peak integration. The assigned protons are color-coded as in (d). 'n' represents the number of repeating units in the oligomers.  $n = 0$  to 5 indicate oligomers 3-**mer** to 8-**mer**, respectively. (e) Side view of the energy-minimized molecular models of the 2-**mer**, 4-**mer**, and 8-**mer** using the MMFFs shown in tube representation. Hydrogen atoms are omitted for clarity. Length and molecular weight are indicated. Models for other oligomers are given in the ESI.†



creating only one isomer by simply adjusting side chains would be remarkable.

To assess the photo-oligomerization process, macrocycle **1** was irradiated with a broad wavelength range of 320–390 nm, matching well with its absorption maxima (Fig. S5†), for three hours under anaerobic conditions in chloroform (Scheme S4†).  $^1\text{H}$ -NMR spectra were recorded at intervals, revealing significant changes compared to the initial spectrum and the emergence of several new signals (Fig. S6†). Notably, resonances in the range of 5.0–5.4 ppm, attributed to H10\* (Fig. 2c), indicated the progress of [4 + 4] cycloaddition.<sup>59–61</sup> MALDI-TOF mass spectrometry confirmed the formation of higher oligomers (Fig. S7†), which were separated by recycling GPC (Fig. S8†). After three cycles, peaks all the way to the **8-mer** can be distinguished (Fig. 2a). The gradual decrease of peak intensity with increasing size suggests a lower reactivity as the oligomer size increases. One can observe that longer irradiation times lead to an increasing proportion of higher oligomers (Fig. S9†) but may cause thermal decomposition due to sample heating in our setup. However, this issue could be resolved by irradiating at lower temperatures. Each compound from the **2-mer** to the **8-mer** was isolated and identified using  $^1\text{H}$  NMR and mass spectrometry (Fig. S10–S23†).

All oligomeric species were found to be soluble in chloroform.  $^1\text{H}$ -DOSY (diffusion ordered spectroscopy) NMR analysis (Fig. S24–S29†) of **1** and the **2–6-mers** showed that the oligomer diffusion coefficients decreased linearly with increasing their size (Fig. 2b). Using the Stokes–Einstein equation, we estimated their hydrodynamic radii to be 1.3, 1.5, 1.8, 2.1, 2.7, and 3.4 nm, respectively. This trend is in agreement with the theoretical radius of the oligomers (Fig. 2b). The well-resolved  $^1\text{H}$ -NMR resonances in  $\text{CDCl}_3$  (Fig. 2c) were consistent with the structures assigned based on mass spectrometry. In contrast to monomeric macrocycle **1**, which displays a single amide resonance, the **2-mer** showed two amide signals at 11.35 and 10.55 ppm, corresponding to terminal and central amide protons, respectively. Interestingly, the spectrum of the **3-mer** showed only one set of sharp signals, suggesting that only one of the two possible isomers had formed. For all the longer oligomers, three types of NH amide signals with varying intensities were observed. Based on symmetry, these signals can be assigned to terminal NHs (yellow, Fig. 2c and d), those neighboring the terminal NHs (magenta), and all the remaining central amides (pink and cyan). For the **4-mer**, two types of central NHs can be distinguished (pink and cyan), attesting to the sensitivity of NMR in distinguishing small differences in the environment. We thus infer that the single set of sharp resonances for all compounds reflects the presence of only one isomer, *i.e.*, other isomers would give rise to some distinct resonances should they be present. The chemical shift values of the amide signals remain relatively constant for the higher oligomers. Only the relative intensity of the central amide signal varies. This indicates that central amides are all in a similar environment, consistent with the oligomers remaining in a rigid structure. The signals in the 5–5.4 ppm region correspond to the H10\* protons of diazaanthracenes

after the [4 + 4] cycloaddition. The peak integration of each signal allowed us to confirm the oligomer length using the terminal resonance as a reference (Fig. 2c, yellow).

Since growing single crystals suitable for the X-ray analysis of the oligomers has so far eluded us, we used molecular modeling to gain structural insights (Fig. 2e, and Fig. S30–S36†). The models revealed rigid, ladder-shaped structures with an average plane-to-plane separation (*i.e.* step size) of 4.6 Å (Fig. S37†) and a length of up to 10 nm for the **8-mer**. The molecular lengths of the oligomers predicted by these models closely match the hydrodynamic radii derived from the DOSY experiments (Fig. 2b).

The oligomers are thermally quite stable up to 353 K with no noticeable changes over three days. However, beyond this temperature, they started decomposing into smaller oligomers.

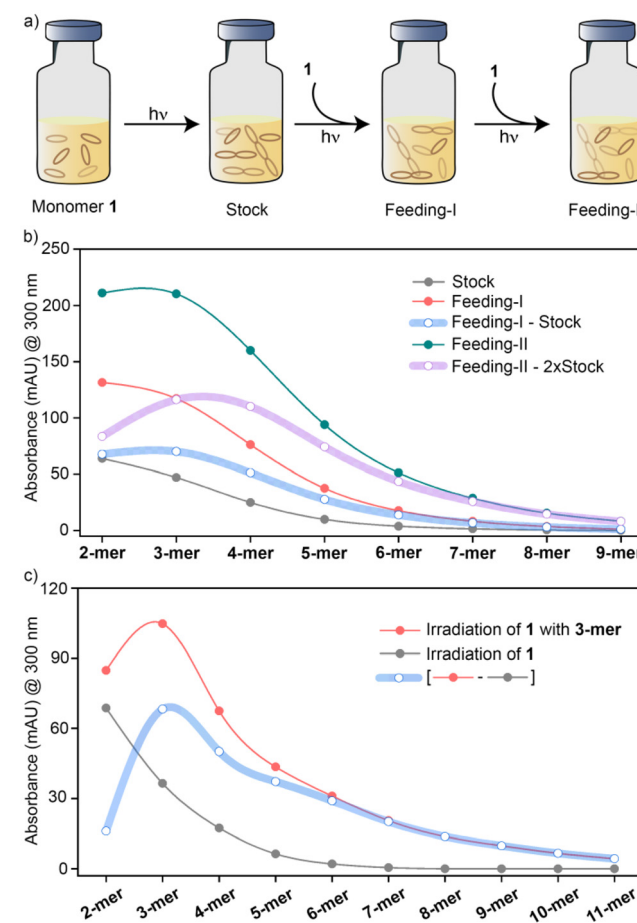


**Fig. 3** (a) Schematic representation of multicycle oligomerization. Monomer **1** was initially irradiated to obtain a mixture of oligomers. Then, fresh monomers were added to obtain higher oligomers and enhance their proportions. (b) The plot summarizes the evolution of oligomers after every feeding step. The proportion of the oligomers is normalized against the initial irradiation step to indicate a significant enhancement in the oligomer concentration. (c) Evolution of oligomers when irradiation of monomers was performed in the presence of a **3-mer**. The normalized data with respect to the oligomers formed in the absence of the **3-mer** showed a significant role in forming higher oligomers. The lines connecting points are for visual guidance.



To achieve complete thermal reversibility, the **4-mer** was heated at 393 K in 1,1,2,2-tetrachloroethane over a period of 60 h (Fig. S38†). <sup>1</sup>H NMR analyses performed at intervals revealed the transient appearance of the **2-mer** and **3-mer**, thus hinting at a gradual degradation of the **4-mer** (Fig. S39†). Attempts to reverse the cycloaddition using light irradiation at 254 nm were ineffective.

To assess how a given oligomer could be further elongated and to decipher the mechanism of the formation of long oligomers, we conducted feeding experiments in which fresh macrocycle **1** was added at intervals during the reaction. Initially, **1** was irradiated in chloroform for 1 h to generate a mixture of oligomers. Subsequently, two feeding cycles were performed with the addition of fresh **1**, followed by irradiation. The evolution of the oligomer formation was monitored by GPC after each cycle (Fig. S40 and S41†), showing a significant increase in the proportion of higher oligomers (Fig. 3b), despite **1** being capable of independent oligomerization in every feeding cycle. The normalized data indicate the influence of the parent oligomers, *i.e.*, the oligomers present before fresh macrocycle monomers were added, in promoting the formation of higher oligomers. This is consistent with the oligomers reacting slowly with each other while they can still react with the monomer and undergo elongation. Consistently, we observed that performing the photo oligomerization of **1** in the presence of the **3-mer** facilitated the formation of higher oligomers, such as a **10-mer** and **11-mer** (Fig. S42 & S43†), which could not be achieved by irradiating **1** alone in the same timeframe. Moreover, we found that when we directly irradiated a preformed **2-mer** over one hour in chloroform, oligomers of the **2-mer**, such as the **4-mer**, **6-mer**, and **8-mer**, were formed in higher proportion, but odd-numbered oligomers also formed (Fig. S44–S46†), likely due to thermal reversibility caused by heat due to the irradiation. These experiments demonstrate that the oligomers are sufficiently photoreactive to undergo further oligomerization in the presence of monomers.

## Conclusions

In conclusion, we have used a simple [4 + 4] cycloaddition reaction to photo-oligomerize a planar macrocycle containing light-sensitive diazaanthracene moieties. By properly choosing the solubilizing side chains, we were able to control the stereo-selectivity to obtain discrete ladder-like oligomers out of many other possible isomers. Oligomers up to the **8-mer** were easily isolated by GPC and characterized by NMR and mass spectrometry. The ability to obtain large oligomers with molecular weights over 10 kDa in a single-step photoirradiation is rare. We demonstrated that these oligomers remained sufficiently reactive to further react with fresh monomers to form even longer oligomers. The oligomers also exhibit thermal reversibility, returning to monomers along the same pathway. This approach holds promise for synthesizing other functional oligomers from different photoresponsive monomers.

## Author contributions

B. G., Y. F., and I. H. conceived the project. J. M. K. planned and conducted the experiments. B. G. supervised the research, performed analysis, and wrote the original draft of the manuscript. Y. F and I. H. provided critical feedback during the whole process and edited the manuscript.

## Data availability

The data supporting this article have been included as part of the ESI.†

## Conflicts of interest

There are no conflicts to declare.

## Acknowledgements

We thank Shiv Nadar Institution of Eminence (SNIoE), Delhi NCR, and the Anusandhan National Research Foundation (ANRF), Govt. of India (SRG/2022/000678), for financial support and the DST-FIST scheme for the MALDI facility.

## References

- 1 A. P. Côté, A. I. Benin, N. W. Ockwig, M. O’Keeffe, A. J. Matzger and O. M. Yaghi, Porous, Crystalline, Covalent Organic Frameworks, *Science*, 2005, **310**, 1166–1170.
- 2 S. Kandambeth, K. Dey and R. Banerjee, Covalent Organic Frameworks: Chemistry beyond the Structure, *J. Am. Chem. Soc.*, 2019, **141**, 1807–1822.
- 3 A. Basak, S. Karak and R. Banerjee, Covalent Organic Frameworks as Porous Pigments for Photocatalytic Metal-Free C–H Borylation, *J. Am. Chem. Soc.*, 2023, **145**, 7592–7599.
- 4 S. Paul, M. Gupta, A. K. Mahato, S. Karak, A. Basak, S. Datta and R. Banerjee, Covalent Organic Frameworks for the Purification of Recombinant Enzymes and Heterogeneous Biocatalysis, *J. Am. Chem. Soc.*, 2024, **146**, 858–867.
- 5 F. Beuerle and B. Gole, Covalent Organic Frameworks and Cage Compounds: Design and Applications of Polymeric and Discrete Organic Scaffolds, *Angew. Chem., Int. Ed.*, 2018, **57**, 4850–4878.
- 6 B. Gole, V. Stepanenko, S. Rager, M. Grüne, D. D. Medina, T. Bein, F. Würthner and F. Beuerle, Microtubular Self-Assembly of Covalent Organic Frameworks, *Angew. Chem., Int. Ed.*, 2018, **57**, 846–850.
- 7 Y. Fang, Y. Liu, H. Huang, J. Sun, J. Hong, F. Zhang, X. Wei, W. Gao, M. Shao, Y. Guo, Q. Tang and Y. Liu, Design and synthesis of broadband absorption covalent organic framework for efficient artificial photocatalytic amine coupling, *Nat. Commun.*, 2024, **15**, 4856.



8 M. O'Shaughnessy, J. Glover, R. Hafizi, M. Barhi, R. Clowes, S. Y. Chong, S. P. Argent, G. M. Day and A. I. Cooper, Porous isoreticular non-metal organic frameworks, *Nature*, 2024, **630**, 102–108.

9 D. He, H. Ji, T. Liu, M. Yang, R. Clowes, M. A. Little, M. Liu and A. I. Cooper, Self-Assembly of Chiral Porous Metal-Organic Polyhedra from Trianglsalen Macrocycles, *J. Am. Chem. Soc.*, 2024, **146**, 17438–17445.

10 B. P. Benke, T. Kirschbaum, J. Graf, J. H. Gross and M. Mastalerz, Dimeric and trimeric catenation of giant chiral [8 + 12] imine cubes driven by weak supramolecular interactions, *Nat. Chem.*, 2023, **15**, 413–423.

11 P. Wagner, F. Rominger, J. H. Gross and M. Mastalerz, Solvent-Controlled Quadruple Catenation of Giant Chiral [8 + 12] Salicylimine Cubes Driven by Weak Hydrogen Bonding, *Angew. Chem., Int. Ed.*, 2023, **62**, e202217251.

12 P. Wagner, F. Rominger, W.-S. Zhang, J. H. Gross, S. M. Elbert, R. R. Schröder and M. Mastalerz, Chiral Self-sorting of Giant Cubic [8 + 12] Salicylimine Cage Compounds, *Angew. Chem., Int. Ed.*, 2021, **60**, 8896–8904.

13 M. Liu, L. Zhang, M. A. Little, V. Kapil, M. Ceriotti, S. Yang, L. Ding, D. L. Holden, R. Balderas-Xicohténcatl, D. He, R. Clowes, S. Y. Chong, G. Schütz, L. Chen, M. Hirscher and A. I. Cooper, Barely porous organic cages for hydrogen isotope separation, *Science*, 2019, **366**, 613–620.

14 C. Liu, K. Liu, C. Wang, H. Liu, H. Wang, H. Su, X. Li, B. Chen and J. Jiang, Elucidating heterogeneous photocatalytic superiority of microporous porphyrin organic cage, *Nat. Commun.*, 2020, **11**, 1047.

15 S. M. Elbert, O. T. A. Paine, T. Kirschbaum, M. P. Schuldt, L. Weber, F. Rominger and M. Mastalerz, A Negatively Curved Nanographene with Four Embedded Heptagons, *J. Am. Chem. Soc.*, 2024, **146**, 27324–27334.

16 X. Yang, M. Brückner, F. Rominger, T. Kirschbaum and M. Mastalerz, Dispersion-driven formation of chiral twisted PAH double helices, *Chem*, 2024, **10**, 832–842.

17 R. Roy, C. Brouillac, E. Jacques, C. Quinton and C. Porié,  $\pi$ -Conjugated Nanohoops: A New Generation of Curved Materials for Organic Electronics, *Angew. Chem., Int. Ed.*, 2024, **63**, e202402608.

18 H. Omachi, T. Nakayama, E. Takahashi, Y. Segawa and K. Itami, Initiation of carbon nanotube growth by well-defined carbon nanorings, *Nat. Chem.*, 2013, **5**, 572–576.

19 Y. Li, A. Yagi and K. Itami, Synthesis of Highly Twisted, Nonplanar Aromatic Macrocycles Enabled by an Axially Chiral 4,5 Diphenylphenanthrene Building Block, *J. Am. Chem. Soc.*, 2020, **142**, 3246–3253.

20 H. Shudo, M. Kuwayama, M. Shimasaki, T. Nishihara, Y. Takeda, N. Mitoma, T. Kuwabara, A. Yagi, Y. Segawa and K. Itami, Perfluorocycloparaphenylenes, *Nat. Commun.*, 2022, **13**, 3713.

21 K. Shoyama and F. Würthner, Synthesis of a Carbon Nanocone by Cascade Annulation, *J. Am. Chem. Soc.*, 2019, **141**, 13008–13012.

22 M. Mahl, M. A. Niyas, K. Shoyama and F. Würthner, Multilayer stacks of polycyclic aromatic hydrocarbons, *Nat. Chem.*, 2022, **14**, 457–462.

23 Q. Huang, G. Zhuang, M. Zhang, J. Wang, S. Wang, Y. Wu, S. Yang and P. Du, A Long  $\pi$ -Conjugated Poly(*para*-Phenylene)-Based Polymeric Segment of Single-Walled Carbon Nanotubes, *J. Am. Chem. Soc.*, 2019, **141**, 18938–18943.

24 Y. Xu, S. Gsänger, M. B. Minameyer, I. Imaz, D. Maspoch, O. Shyshov, F. Schwer, X. Ribas, T. Drewello, B. Meyer and M. von Delius, Highly Strained, Radially  $\pi$ -Conjugated Porphyrinylene Nano hoops, *J. Am. Chem. Soc.*, 2019, **141**, 18500–18507.

25 J. Xu, K. Jung, A. Atme, S. Shanmugam and C. Boyer, A Robust and Versatile Photoinduced Living Polymerization of Conjugated and Unconjugated Monomers and Its Oxygen Tolerance, *J. Am. Chem. Soc.*, 2014, **136**, 5508–5519.

26 X. Hu, G. Szczepaniak, A. Lewandowska-Andraloje, J. Jeong, B. Li, H. Murata, R. Yin, A. M. Jazani, S. R. Das and K. Matyjaszewski, Red-Light-Driven Atom Transfer Radical Polymerization for High-Throughput Polymer Synthesis in Open Air, *J. Am. Chem. Soc.*, 2023, **145**, 24315–24327.

27 M. Chen, M. Zhong and J. A. Johnson, Light-Controlled Radical Polymerization: Mechanisms, Methods, and Applications, *Chem. Rev.*, 2016, **116**, 10167–10211.

28 C. Förster and A. Andrieu-Brunsen, Recent developments in visible light induced polymerization towards its application to nanopores, *Chem. Commun.*, 2023, **59**, 1554–1568.

29 L. Dou, Y. Zheng, X. Shen, G. Wu, K. Fields, W.-C. Hsu, H. Zhou, Y. Yang and F. Wudl, Single-crystal linear polymers through visible light-triggered topochemical quantitative polymerization, *Science*, 2014, **343**, 272–277.

30 C. Sun, J. J. Oppenheim, G. Skorupskii, L. Yang and M. Dincă, Reversible topochemical polymerization and depolymerization of a crystalline 3D porous organic polymer with C–C bond linkages, *Chem*, 2022, **8**, 3215–3224.

31 R. Z. Lange, G. Hofer, T. Weber and A. D. Schlüter, A Two-Dimensional Polymer Synthesized through Topochemical [2 + 2]-Cycloaddition on the Multigram Scale, *J. Am. Chem. Soc.*, 2017, **139**, 2053–2059.

32 K. Hema, A. Ravi, C. Raju, J. R. Pathan, R. Rai and K. M. Sureshan, Topochemical polymerizations for the solid-state synthesis of organic polymers, *Chem. Soc. Rev.*, 2021, **50**, 4062–4099.

33 B. Bibal, C. Mongin and D. M. Bassani, Template effects and supramolecular control of photoreactions in solution, *Chem. Soc. Rev.*, 2014, **43**, 4179–4198.

34 V. Ramamurthy and J. Sivaguru, Supramolecular Photochemistry as a Potential Synthetic Tool: Photocycloaddition, *Chem. Rev.*, 2016, **116**, 9914–9993.

35 K. Biradha and R. Santra, Crystal engineering of topochemical solid state reactions, *Chem. Soc. Rev.*, 2013, **42**, 950–967.

36 H. Bouas-Laurent, A. Castellan, J.-P. Desvergne and R. Lapouyade, Photodimerization of anthracenes in fluid solution: structural aspects, *Chem. Soc. Rev.*, 2000, **29**, 43–55.



37 H. Bouas-Laurent, A. Castellan, J.-P. Desvergne and R. Lapouyade, Photodimerization of anthracenes in fluid solutions: (part 2) mechanistic aspects of the photocycloaddition and of the photochemical and thermal cleavage, *Chem. Soc. Rev.*, 2001, **30**, 248–263.

38 Z.-A. Huang, C. Chen, X.-D. Yang, X.-B. Fan, W. Zhou, C.-H. Tung, L.-Z. Wu and H. Cong, Synthesis of Oligoparaphenylenes-Derived Nanohoops Employing an Anthracene Photodimerization–Cycloreversion Strategy, *J. Am. Chem. Soc.*, 2016, **138**, 11144–11147.

39 J. Tanabe, D. Taura, N. Ousaka and E. Yashima, Chiral Template-Directed Regio-, Diastereo-, and Enantioselective Photodimerization of an Anthracene Derivative Assisted by Complementary Amidinium–Carboxylate Salt Bridge Formation, *J. Am. Chem. Soc.*, 2017, **139**, 7388–7398.

40 Y. Kawanami, S. Y. Katsumata, M. Nishijima, G. Fukuhara, K. Asano, T. Suzuki, C. Yang, A. Nakamura, T. Mori and Y. Inoue, Supramolecular Photochirogenesis with a Higher-Order Complex: Highly Accelerated Exclusively Head-to-Head Photocyclodimerization of 2-Anthracenecarboxylic Acid via 2:2 Complexation with Prolinol, *J. Am. Chem. Soc.*, 2016, **138**, 12187–12201.

41 A. Nakamura and Y. Inoue, Supramolecular Catalysis of the Enantiodifferentiating [4 + 4] Photocyclodimerization of 2-Anthracenecarboxylate by  $\gamma$ -Cyclodextrin, *J. Am. Chem. Soc.*, 2003, **125**, 966–972.

42 J. Yao, Z. Yan, J. Ji, W. Wu, C. Yang, M. Nishijima, G. Fukuhara, T. Mori and Y. Inoue, Ammonia-Driven Chirality Inversion and Enhancement in Enantiodifferentiating Photocyclodimerization of 2-Anthracenecarboxylate Mediated by Diguanidino- $\gamma$ -cyclodextrin, *J. Am. Chem. Soc.*, 2014, **136**, 6916–6919.

43 M. Nishijima, T. Wada, T. Mori, T. C. S. Pace, C. Bohne and Y. Inoue, Highly Enantiomeric Supramolecular [4 + 4] Photocyclodimerization of 2-Anthracenecarboxylate Mediated by Human Serum Albumin, *J. Am. Chem. Soc.*, 2007, **129**, 3478–3479.

44 X. Wei, J. Ji, Y. Nie, L. Tang, M. Rao, X. Wang, W. Wu, D. Su, Z. Zhong and C. Yang, Synthesis of cyclodextrin derivatives for enantiodifferentiating photocyclodimerization of 2-anthracenecarboxylate, *Nat. Protoc.*, 2022, **17**, 2494–2516.

45 P. Kissel, D. J. Murray, W. J. Wulf Lange, V. J. Catalano and B. T. King, A nanoporous two-dimensional polymer by single-crystal-to-single-crystal photopolymerization, *Nat. Chem.*, 2014, **6**, 774–778.

46 R. Bhola, P. Payamyar, D. J. Murray, B. Kumar, A. J. Teator, M. U. Schmidt, S. M. Hammer, A. Saha, J. Sakamoto, A. D. Schlüter and B. T. King, A two-dimensional polymer from the anthracene dimer and triptycene motifs, *J. Am. Chem. Soc.*, 2013, **135**, 14134–14141.

47 M. J. Kory, M. Worle, T. Weber, P. Payamyar, S. W. van de Poll, J. Dshemuchadse, N. Trapp and A. D. Schlüter, Gram-scale synthesis of two-dimensional polymer crystals and their structure analysis by X-ray diffraction, *Nat. Chem.*, 2014, **6**, 779–784.

48 M. Servalli, N. Trapp and A. D. Schlüter, Single-Crystal-to-Single-Crystal (SCSC) Linear Polymerization of a Desymmetrized Anthraphane, *Chem. – Eur. J.*, 2018, **24**, 15003–15012.

49 L. Grossmann, B. T. King, S. Reichlmaier, N. Hartmann, J. Rosen, W. M. Heckl, J. Björk and M. Lackinger, On-surface photopolymerization of two-dimensional polymers ordered on the mesoscale, *Nat. Chem.*, 2021, **13**, 730–736.

50 K. Kristinaityte, A. Mames, M. Pietrzak, F. F. Westermair, W. Silva, R. M. Gschwind, T. Ratajczyk and M. Urbańczyk, Deeper Insight into Photopolymerization: The Synergy of Time-Resolved Nonuniform Sampling and Diffusion NMR, *J. Am. Chem. Soc.*, 2022, **144**, 13938–13945.

51 R. Y. Liu, S. Guo, S.-X. L. Luo and T. M. Swager, Solution-processable microporous polymer platform for heterogenization of diverse photoredox catalysts, *Nat. Commun.*, 2022, **13**, 2775.

52 C. L. Anderson, H. Li, C. G. Jones, S. J. Teat, N. S. Settineri, E. A. Dailing, J. Liang, H. Mao, C. Yang, L. M. Klivansky, X. Li, J. A. Reimer, H. M. Nelson and Y. Liu, Solution-processable and functionalizable ultra-high molecular weight polymers via topochemical synthesis, *Nat. Commun.*, 2021, **12**, 6818.

53 A. Wang, R. Tan, C. Breakwell, X. Wei, Z. Fan, C. Ye, R. Malpass-Evans, T. Liu, M. A. Zwijnenburg, K. E. Jeffs, N. B. McKeown, J. Chen and Q. Song, Solution-Processable Redox-Active Polymers of Intrinsic Microporosity for Electrochemical Energy Storage, *J. Am. Chem. Soc.*, 2022, **144**, 17198–17208.

54 H. Ihmels, C. J. Mohrschladt, A. Schmitt, M. Bressanini, D. Leusser and D. Stalke, Highly Regioselective Solid-State Photodimerization of Naphthoquinolizinium Salts, *Eur. J. Org. Chem.*, 2002, 2624–2632.

55 D. Jouvenot, E. C. Glazer and Y. Tor, Photodimerizable ditopic ligand, *Org. Lett.*, 2006, **8**, 1987–1990.

56 E. Berni, C. Dolain, B. Kauffmann, J.-M. Léger, C. Zhan and I. Huc, Expanding the Registry of Aromatic Amide Foldamers: Folding, Photochemistry and Assembly Using Diaza-anthracene Units, *J. Org. Chem.*, 2008, **73**, 2687–2694.

57 M. Li, A. D. Schlüter and J. Sakamoto, Solid-State Photopolymerization of a Shape-Persistent Macrocyclic with Two 1,8-Diazaanthracene Units in a Single Crystal, *J. Am. Chem. Soc.*, 2012, **134**, 11721–11725.

58 P. Payamyar, M. Servalli, T. Hungerland, A. P. Schütz, Z. Zheng, A. Borgschulte and A. D. Schlüter, Approaching Two-Dimensional Copolymers: Photoirradiation of Anthracene- and Diaza-Anthracene-Bearing Monomers in Langmuir Monolayers, *Macromol. Rapid Commun.*, 2015, **36**, 151–158.

59 B. Gole, B. Kauffmann, V. Maurizot, I. Huc and Y. Ferrand, Light-Controlled Conformational Switch of an Aromatic Oligoamide Foldamer, *Angew. Chem., Int. Ed.*, 2019, **58**, 8063–8067.

60 B. Gole, B. Kauffmann, A. Tron, V. Maurizot, N. McClenaghan, I. Huc and Y. Ferrand, Selective and



Cooperative Photocycloadditions within Multistranded Aromatic Sheets, *J. Am. Chem. Soc.*, 2022, **144**, 6894–6906.

61 C. Yao, B. Gole, A. T. Bui, B. Kauffmann, I. Huc, N. D. McClenaghan and Y. Ferrand, Photon-gated foldaxane assembly/disassembly, *Chem. Commun.*, 2024, **60**, 8415–8418.

62 M. Jaymand, Recent progress in the chemical modification of syndiotactic polystyrene, *Polym. Chem.*, 2014, **5**, 2663–2690.

63 T. Ikai, T. Yoshida, K. Shinohara, T. Taniguchi, Y. Wada and T. M. Swager, Triptycene-Based Ladder Polymers with One-Handed Helical Geometry, *J. Am. Chem. Soc.*, 2019, **141**, 4696–4703.